DOI: 10.1002/ejic.200601218

Order and Disorder in Cluster Phases – The Case of $La_{\approx 0.7}(Al_{\approx 0.1}I_{\approx 0.9})$

Lorenz Kienle,*[a] Oliver Oeckler,[b] Thomas Weber,[c] Viola Duppel,[a] Hansjürgen Mattausch,[a] and Arndt Simon[a]

Keywords: Electron microscopy / X-ray diffraction / Rare earth metal compounds / Clusters / Halides / Disorder

The structure of the new partially ordered cluster phase $La_{0.69(1)}(Al_{0.12(1)}I_{0.88(1)})$ was determined by a combined methodical approach of electron microscopy techniques and X-ray diffraction. The structure is derived from the Gd_3CCl_3-type and ca. 50 % of the cluster positions in this structure type are occupied. The majority of the clusters are condensed via common edges, however, the degree of cluster condensation is low. The arrangement of neighboring clusters is comparable to chemically related, but strongly disordered cluster phases.

Introduction

Many low-valent compounds of rare earth metals (Ln) are composed of discrete or condensed clusters[1] of the Ln_6ZX_{12}-type (X = Cl, Br, I). Endohedral species Z (Z = B, C, C_2, etc.) centering the octahedral Ln_6 core stabilize the valence electron-poor clusters.[2] Most phases with isolated or condensed Ln_6ZX_{12}-type clusters show a topological relationship with the NaCl-type structure thus following the general remark that rocksalt is everywhere.[3] The Z atoms replace a fraction of the X atoms on the anion positions, whereas Ln atoms and voids are located on the cation positions, and all Z atoms are surrounded by six Ln neighbors. The ratio Ln/Z determines the degree of cluster condensation with the maximum value of 6 for phases with discrete Ln_6ZX_{12} clusters as in Zr_6CI_{12}[4] and decreased ratios for the condensed cluster phases, e.g. Ln/Z = 5 for $La_{10}(C_2)_2I_{18}$[5] containing double octahedra. As a rule, neighboring Ln_6 octahedra are connected via edges both in ordered and disordered phases. Well-documented examples for the first are the triple Ln_{14} octahedra in $Ln_{14}(C_2)_3I_{20}$ (Ln = La, Ce; Ln/Z = 4.67)[6] and the linear chain of octahedra found in Sc_4CCl_6 (Ln/Z = 4).[7] Examples for the latter are $Ln_{13}B_3Br_{18}$ (Ln = Gd, Tb)[8] and $Ce_{29}Al_{14}I_{28}$[9] where discrete Ln_{10} double octahedra are ordered in layers which, however, exhibit stacking disorder. The disordered intergrowth phases $Ln_{4n+2}(C_2)_nI_{5n+5}$[10] contain layers of linear oligomers with distinct numbers (*n*) of condensed octahedra.

Recently, we analyzed the connectivity of clusters in the highly disordered phase $La_{0.70}(Al_{0.14}I_{0.86})$ (**1**)[11] with average NaCl-type structure. Here, we report on $La_{0.70}(Al_{0.12}I_{0.88})$ (**2**) which is the first partially ordered cluster phase occurring in the system La–Al–I. In the context of the following, the structure of Gd_3CCl_3[12] is of particular importance (Ca_3PI_3-type,[13] $I4_132$). Each octahedron of the latter is connected to three neighboring ones; see Figure 1, producing a characteristic quadratic or hexagonal pattern of clusters in projections along <100> and

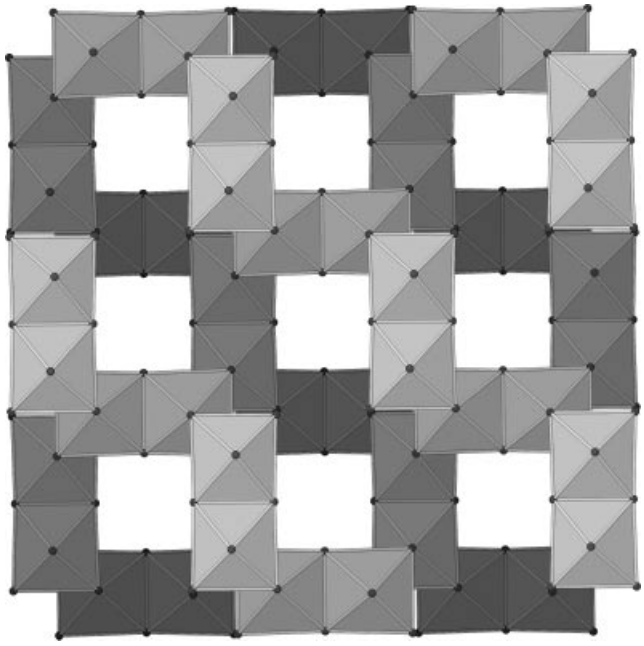

Figure 1. CGd_6 clusters in the structure of Gd_3CCl_3 along <100>, Cl atoms are omitted.

[a] Max-Planck-Institut für Festkörperforschung
Heisenbergstrasse 1, 70569 Stuttgart, Germany
Fax: +49-711-6891091
E-mail: L.Kienle@fkf.mpg.de
[b] Department Chemie und Biochemie der Ludwig-Maximilians-Universität
Butenandtstrasse 5–13(D), 81377 München, Germany
[c] Laboratorium für Kristallographie, ETH Hönggerberg
Wolfgang-Pauli-Strasse 10, 8093 Zürich, Switzerland

<111>, respectively. All known representatives of this structure type, including distorted ones,[14] are fully ordered.

Results and Discussion

Despite the highly disordered real structure, neighboring clusters in **1** are far from a random arrangement. A structure refinement based on the intensity of the diffuse X-ray scattering had allowed the evaluation of relative cluster positions, indicating the presence of edge-condensed La_6 octahedra as expected from the ratio Ln/Z = 5, however, only as a small fraction. Crystals of **1** exhibit halo-shaped diffuse scattering around the Bragg reflections of electron and X-ray diffraction patterns. The new variant, **2** shows a segregation of the diffuse scattering into superstructure reflections indicating partial long-range ordering. The different degrees of structural disorder in **1** and **2** are exemplified by the SAED (selected area electron diffraction) patterns and electron micrographs of Figure 2. Both crystals were aligned along zone axis <111>, referring to the common NaCl-type subcell. The high resolution image for **1** (Figure 2, a) shows a strongly disordered, but non-random arrangement of dark and bright spots. The interpretation by simulated micrographs is based on the structural model derived from the diffuse X-ray scattering.[11] For $\Delta f \approx -70$ nm, low values of the projected potential produce dark spots, corresponding to the preferred cluster arrangement which leads to a superposition of Al atoms and voids along <111>, and bright spots represent high values of the projected potential resulting from <111> rows of La and I atoms. Following this analysis, **1** is characterized by pronounced correlations of the cluster positions. The interrelation of projected potential and image contrast is straightforward for all defocus values not only for Scherzer focus. The preferred cluster arrangement of **1** is imaged in the form of dark spots each surrounded by a hexagon of bright spots. Such hexagons can be seen in Figure 2 (a) bottom (see marks), however, they do not produce a periodic pattern due to the lack of perfect long range order in **1**. This contrasts the partially ordered crystallites of **2**, where ordering of the hexagons in {111} is observed, see Figure 2 (b) bottom. At the first glance, the HRTEM image seems to be entirely periodic, however, significant variations of the spot intensities are evident which disrupt the periodicity. In some cases, the partial order can also be demonstrated by faint diffuse intensities in Fourier transforms of HRTEM micrographs as seen in the electron-diffraction patterns (see Figure 2, b, top). SAED as well as corresponding zero layer X-ray patterns, like those along <100>, exhibit hardly any diffuse scattering. However, this observation does not unambiguously indicate long-range order of the 3D real structure, but a low significance of the disorder in the respective projection. A tilt from the precise zone axis orientation enables one to observe the diffuse intensity, and the existence of disorder becomes evident.

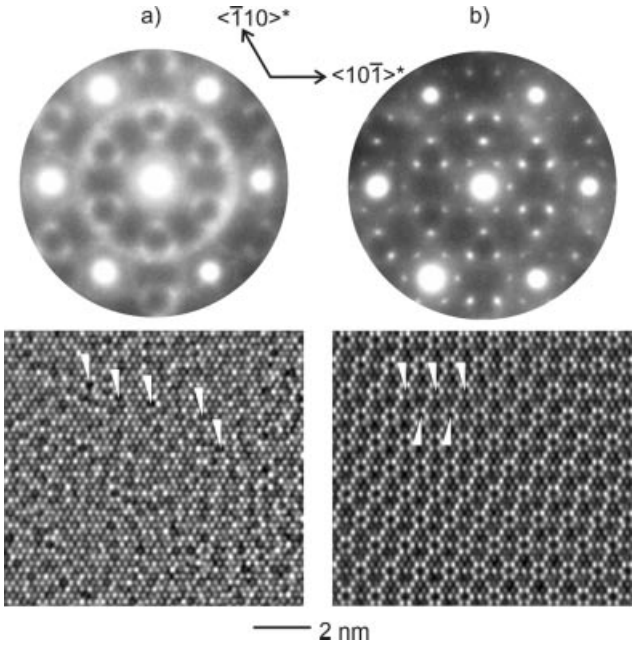

Figure 2. SAED pattern and HRTEM micrograph ($\Delta f \approx -70$ nm) for zone axis <111> recorded on a crystal of **1** (a), and **2** (b).

Such findings were the starting points for an interpretation of HRTEM micrographs and the corresponding SAED patterns of **2** in terms of the 3D structure, and they also entered the X-ray structure analysis. Two important aspects, the chemical composition and an average model need to be taken into account in order to derive a 3D structure of **2** before the real structure can be analyzed in detail. In order to elaborate the specific benefits, the information obtained by both approaches will be asserted separately first and then combined in the conclusion.

Chemical Composition of 2

The chemical composition of **2** was determined by combining SAED and EDX. Both techniques allow nanoprobing and identification, whereas chemical analyses of probably inhomogeneous bulk samples are likely to fail due to averaging. The experimentally determined composition of $La_3I_3Al_2$,[15] taken as the standard, indicates only marginal correction factors as the average of 10 point measurements on 10 crystallites gave La 42.9(1.9) atom-%, Al 28.7(1.4) atom-% and I 28.4(1.0) atom-% (calculated values: 43.0 atom-%, 28.5 atom-%, 28.5 atom-%). For **2** we determined La 41.2(2.6) atom-%, Al 7.1(0.5) atom-% and I 51.7(2.9) atom-% (average of 7 point measurements on 7 crystallites), resulting in a composition $La_{0.70(4)}(Al_{0.12(1)}I_{0.88(5)})$. Point measurements on different regions of the same crystallite lead to variations of the composition within standard deviations.

Symmetry of 2

X-ray measurements on single crystals of **2** yield an average unit cell with cubic metrics. A small amount of dif-

fuse scattering is present. The lattice parameter a = 12.689(1) Å corresponds to a $2a2b2c$ supercell of the NaCl-type structure. This supercell has the Laue symmetry $m\bar{3}m$ and is body-centered. Reflections $h00$ are observed only for $h = 4n$, so the resulting space group is $I4_132$. As even small homogeneous selected areas of the crystallites yield tilting series of SAED patterns consistent with this symmetry, it is clear that the high symmetry is not due to twinning by (pseudo)-merohedry or reticular pseudo-merohedry (e.g. tetragonal with $c' = 2a$). Neither electron nor X-ray diffraction gave any indication of an even larger or not body-centered cell of **2**. Furthermore, the plane symmetry of electron micrographs ($p4mm$ for <100>, $p3m1$ for <111>, $p2mm$ for <110>, cf. Figure 5) in combination with the body-centered lattice is only allowed for the space groups $I432$ and $I4_132$.

Structure Refinement from X-ray Data

For the structure refinement on the basis of X-ray data, diffuse scattering was not taken into account. As both the unit cell parameters and the space group $I4_132$ correspond to the Gd_3CCl_3 type,[12] initial refinements were started from an isotypic and hypothetical La_3I_3Al, although the chemical analysis contradicts this composition. The resulting R value (R_1 = 0.21) was not convincing and the small displacement parameter of Al called for a mixed occupancy of this site by Al and I which was refined to an approximate ratio of 1. Hence, the structure contains only half the amount of La_6Al units as compared to "La_3I_3Al". This does not necessarily lead to a lower La content, because all La atoms in the latter structure type belong to two La_6 octahedra. However, refining the occupancy of the La position yields a value of 87%. The model so far is only an approximation as residual electron density is found in the unoccupied octahedral voids of the Gd_3CCl_3 type, corresponding to ca. 15% occupancy with La. This means that a few cluster centers do not coincide with positions of the Gd_3CCl_3-type. Thus, the structure of **2** can be described as an approximately 50% thinned out variant of this structure type with many shared edges remaining and a few alternative cluster positions occupied. The R values (e.g. R_1 = 0.044) for this structure model are satisfactory, in particular as the reflections to parameters ratio is 26 in spite of some disorder. The refinement in $Im\bar{3}m$ yields about the same R values, however, the degree of disorder is higher and no centrosymmetric structure model can explain the $p3m1$ symmetry of electron micrographs for the <111> zone axis, where one would expect a $p6mm$ symmetry which is clearly absent, cf. Figure 5. For $I432$ which is consistent with the symmetry observed in HRTEM but not with all systematic absences, refinements yield a higher degree of disorder, too. Thus, the structure model derived from "La_3I_3Al" gives the best fit of the data with the highest degree of ordering. Based on the model assumptions, this refinement yields the chemical composition $La_{0.69}(I_{0.88}Al_{0.12})$ for **2** in good agreement with chemical analyses. Details are presented in Table 1, atomic parameters in Table 2.

Table 1. Crystal data of **2**.

Formula	$La_{0.69(1)}(Al_{0.12(1)}I_{0.88(1)})$
Formula weight	210.75 [g mol^{-1}]
Crystal system	cubic
Space group	$I4_132$ (no. 214)
Diffractometer type	Stoe IPDS II
Radiation λ	0.71073 Å (Mo-K_α)
Crystal size	0.15 × 0.12 × 0.08 mm
Lattice parameter	a = 12.689(1) Å
Cell volume	2043.1(3) Å^3
Formula units Z	32
$\rho_{calcd.}$	5.481 g cm^{-3}
$F(000)$	2800.7
μ	21.94 mm^{-1}
Temperature	295(2) K
θ range	2.2°–30°
Reflections measured/observed [$F_o^2 \geq 2\sigma(F_o^2)$]	10634/9055
Independent reflections	505 [R_{int} = 0.062]
Absorption correction	numerical
Min./max. transmission	0.086/0.293
Number of refined parameters/restraints	19/0
Goodness of fit	1.14
R_1/wR_2 (all data)	0.052/0.117
R_1/wR_2 [$F_o^2 \geq 2\sigma(F_o^2)$]	0.044/0.112

Structure Information from Electron Microscopy

In an independent approach, the combination of HRTEM and SAED served to derive structure models and to analyze structural defects of **2**. Particularly for the <111> zone axes, the HRTEM micrographs indicate a separation into high and low values of the projected potential, see text above as well as Figure 3, consistent with a disordered arrangement of clusters in a thinned out Gd_3CCl_3-type structure. The triangles highlight regions with high and low cluster concentration, and the corresponding triangles

Table 2. Atom positions and displacement parameters (in Å^2) for **2** and comparison with the ordered Gd_3CCl_3 structure type.

Atom	Wyck.	x	y	z	Occ.	U_{iso}	U_{11}	$U_{22} = U_{33}$	U_{23}	U_{13}	U_{12}	Occ. in Gd_3CCl_3
La1	24*g*	1/8	0.11684(5)	y + 1/4	0.870(4)	0.0345(4)	0.0301(4)	0.0367(4)	–0.0114(4)	0.0014(2)	$-U_{13}$	1 Gd
La2	8*b*	7/8	7/8	7/8	0.15(1)	0.104(9)	0.104(9)	U_{11}	0.034(10)	U_{23}	U_{23}	0
I1	24*h*	1/8	0.38225(5)	$-y$ + 1/4	1[a]	0.0360(4)	0.0293(4)	0.0394(4)	0.0065(4)	0.0013(2)	U_{13}	1 I
I/Al	8*a*	1/8	1/8	1/8	0.525(8) I 0.475(8) Al	0.0375(8)	0.0375(8)	U_{11}	–0.0123(6)	U_{23}	U_{23}	1 C

[a] Due to the presence of La2 atoms, a small fraction of this position is likely to be occupied by Al, however, this was not significant in refinements.

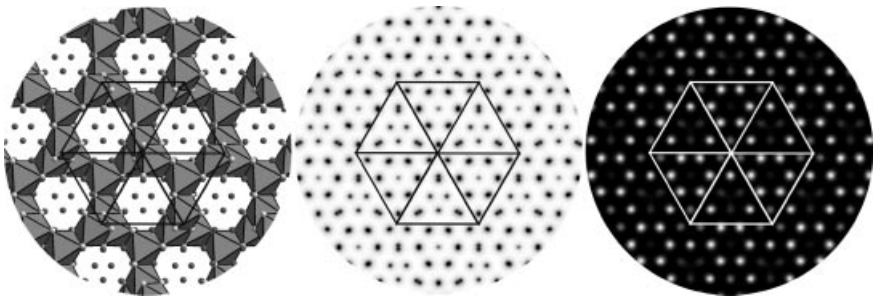

Figure 3. Correlation between projected potential based on the structure model of **2** (see text) and simulated micrograph for <111> (Δf = –70 nm, t = 3.5 nm). From left to right: projection of the structure model, projected potential, simulated micrograph. The triangles highlight regions with high and low cluster concentration.

in the projected potential and in the simulated micrograph give evidence for the experimental significance of such distribution.

In order to check the spatial 3D distribution of the clusters, all fundamental zone axes were investigated in an extended study. Neglecting faint diffuse intensities, experimental and calculated SAED patterns display a convincing agreement for different crystallites (see Figure 4). In addition tilting experiments performed on the same crystallite support the proposed model. As shown by simulations, aggregates of clusters could be identified by SAED and HRTEM; however, the lack of such correlations corresponds to the observed marginal diffuse intensity. Hypothetical structure models of a thinned out and ordered Gd_3CCl_3-type structure were also taken into account. Based on group-subgroup relations several ordering variants are possible, like a hypothetical phase La_5AlI_7 which would contain discrete clusters with edge-sharing double octahedral units. However, such orderings were never observed, even not in nanosized domains.

HRTEM gave additional evidence for the structure of **2**, as demonstrated by the simulated and experimental micrographs of Figure 5. However, a perfect match with simulations is impossible as the averaging is never complete for the transmittable regions of the crystallites. Of course, in very thin regions of the crystallites even an overall disordered distribution of clusters should separate into discernible aggregates. However, in the case of the extremely air-sensitive **2** those regions are already the subject of hydrolysis.

The real structure of **2** is further complicated by the presence of different domains. Firstly, **2** exhibits merohedrally twinned domains and antiphase boundaries, see relative positions of the high- and low intensity spots within the triangles of Figure 6. As the intensity of the spots correlates with the cluster concentration (cf. Figure 3 and Figure 5, bottom), domains with an inverted and shifted (bottom region of Figure 6) and a merely shifted arrangement of the clusters (top region of Figure 6) coexist. The diffraction patterns as well as Fourier transforms of HRTEM micrographs show a complete overlap of the reciprocal lattices for the different domains. Space-averaging of the cluster positions in different domains smaller than the X-ray coherence length could easily explain the detection of clusters on non-cluster positions of the thinned out Gd_3CCl_3-type as determined by XRD.

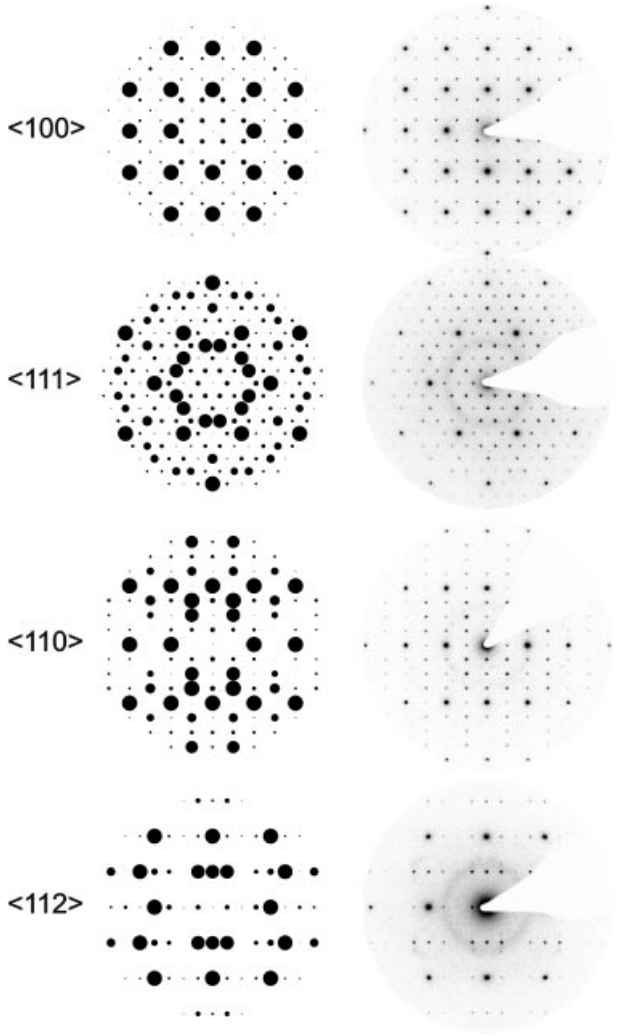

Figure 4. Calculated (left column) and experimental (right column) SAED patterns, zone axes are specified.

Secondly and more rarely, domains of **2** coexist with the domains of a byproduct. The intergrowth can easily by identified by sequentially recorded SAED patterns or the

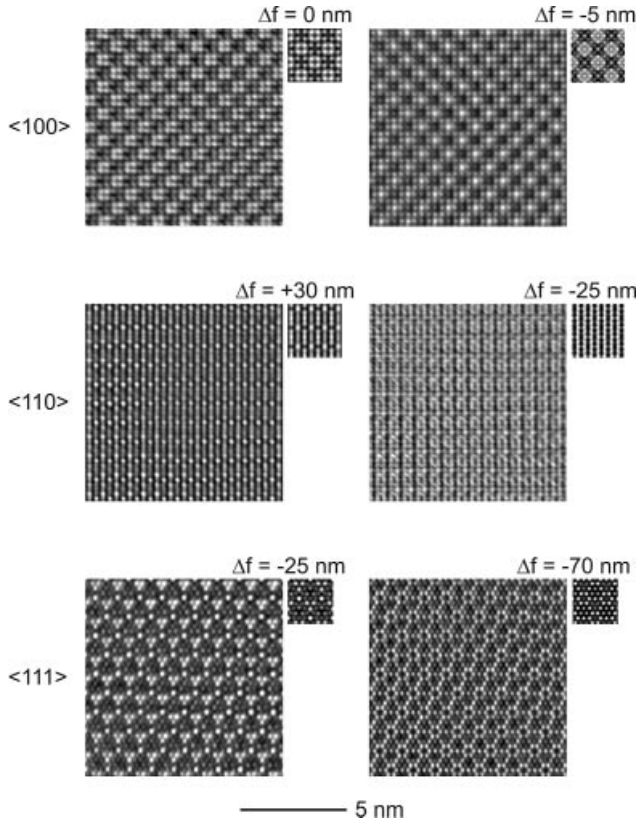

Figure 5. Experimental HRTEM micrographs with simulations for distinct zone axes and defocus values (t<100> = 6.3 nm, t<110> = 5.4 nm and t<111> = 4.4 nm).

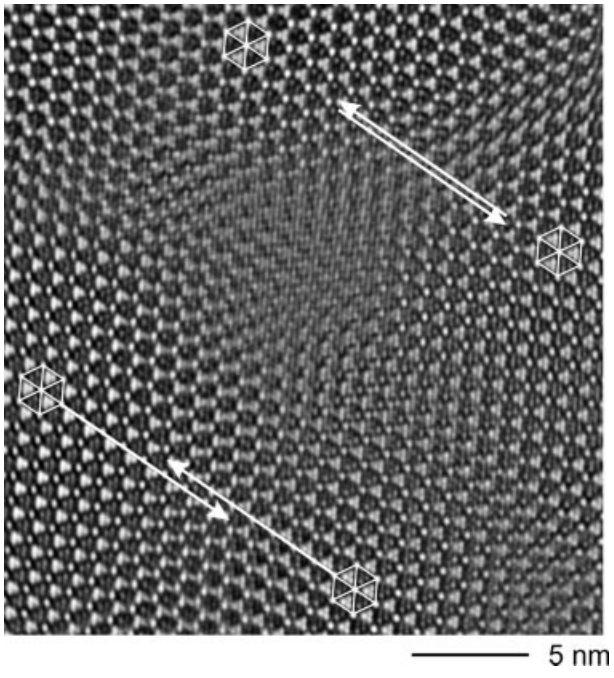

Figure 6. Twin domains (bottom region) and antiphase domains (top region) in **2**. The arrows indicate the shift of the domains.

corresponding superposition patterns, see Figure 7 (a). So far, the composition of the byproduct could not be analyzed reliably by EDX due to shading effects. The *d*-values and intensity distribution of the SAED patterns of the byproduct suggest a phase $La_{7+x}AlI_{12}$ related to Sc_7CI_{12}.[16] Furthermore, some crystallites of the byproduct exhibit the characteristic twinning frequently observed for phases $Ln_{7+x}ZX_{12}$, see superposition pattern in Figure 7 (b). In addition, an intergrowth of this phase and strongly disordered **1** occurs as demonstrated by the characteristic diffuse scattering in the SAED superposition pattern of Figure 7 (c). Hence, the byproduct forms intergrowth phases with both, the chemically related **1** and **2**.

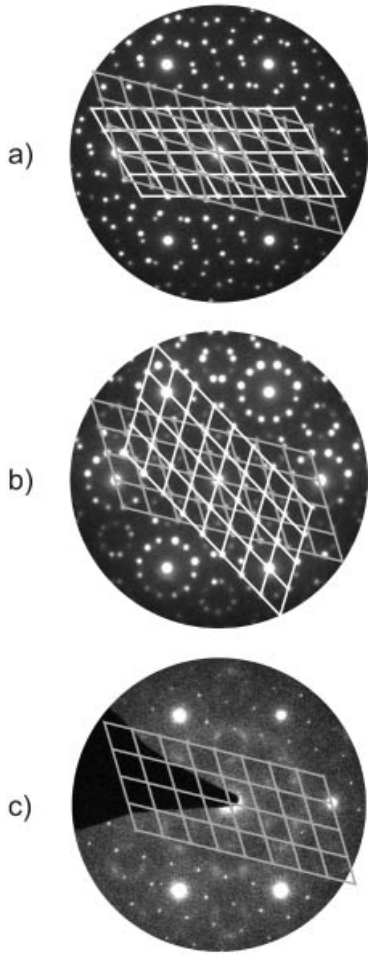

Figure 7. Distinct types of superposition patterns with the common zone axis <111> of **2**. a) Chemical intergrowth of **2** and the byproduct, b) twinning of the byproduct, c) intergrowth of the byproduct and **1**. The grey grids mark the unit cell of the byproduct.

Conclusions

Conventional electron microscopy techniques allow the simultaneous determination of structure and composition of crystals on the nanoscale, however, they do not provide the precise localization of atoms as X-ray diffraction techniques do. Hence, a combined approach is of great value. The structural model for $La_{0.69(1)}(Al_{0.12(1)}I_{0.88(1)})$ determined from electron microscopy was used as the input for an accurate X-ray structure refinement. As X-ray data are

greatly influenced by averaging effects peculiarities of the refined model were then addressed and explained by local investigations in the electron microscope. The strongly disordered phase **1** and the partially ordered phase **2** are close in composition. As expected, they share certain structural properties, however, there are also distinctly different features. Both, the structures of **1** and **2** contain La_6AlI_{12} clusters which are interconnected via I atoms in a rather defined way in spite of the disorder. **1** is arrived at by a systematic cation (La) depletion of a NaCl-type structure leaving the majority of La_6 units in an as far as possible distance from each other. One way of an ordered depletion follows the group-subgroup relation:

$Fm\bar{3}m$ ("Na": *4a*, "Cl": *4b*) $\xrightarrow{t2}$ $F432$ $\xrightarrow{k4}$ $P4_232$ $\xrightarrow{k4,\ a' = 2a}$ $I4_132$ (either La: *24h*, X: *24g*, □: *8a*, Z: *8b*, or La: *24g*, X: *24h*, □: *8b*, Z: *8a*) ending in the Gd_3CCl_3-type structure where close contacts between the metal atoms through edge-sharing of the Ln_6 units are still preserved. In the structure of **2**, this characteristic feature stays when the Gd_3CCl_3-type structure is further thinned out. Hence, the step from **1** via **2** to a Gd_3CCl_3-type structure marks a pathway from a discrete to a condensed cluster phase. As we were not able to change **1** into **2** by extended annealing, it still has to be elucidated which experimental parameters (composition, reaction temperature, etc.) lead along this pathway.

Experimental Section

Synthesis: Powder samples of **2** were prepared by reaction of 500 mg LaI_3, 235 mg AlI_3 and 327 mg La (molar ratio La/Al/I = 18:3:24), pressed to pellets and heated 7 d at 870 °C in closed Ta-capsules.[17] After that the samples were ground and again heated at 900 °C for 8 d. From this batch the crystals were selected for X-ray and HRTEM investigations. All handlings were performed under inert (Ar) gas atmosphere.[18]

X-ray Crystallography: Powder diffractograms were recorded by modified Guinier technique[19] on fine powders sealed in glass capillaries (Cu-$K_{\alpha 1}$, Si as internal standard, Fuji™ film BAS-5000 image plate system). The lattice parameter of the NaCl-type subcell of **2** was determined to $a = 6.326(1)$ Å. Single-crystal X-ray data were collected on a STOE IPDS diffractometer (Mo-K_α radiation). The program package X-Area 1.18 (Stoe, Darmstadt, 2002) was used for data evaluation, SHELX97 was used for structure solution and refinement.[20] Further details of the crystal structure investigation can be obtained from the Fachinformationszentrum Karlsruhe, 76344 Eggenstein-Leopoldshafen, Germany (Fax: +49-7247-808-666; E-mail: crysdata@fiz-karlsruhe.de) on quoting the depository number CSD-417290.

Electron Microscopy and Chemical Analysis: HRTEM and SAED were performed with a Philips CM30ST microscope (300 kV, LaB_6 cathode, $C_S = 1.15$ mm). All manipulations for the preparation and transfer of the sample were carried out under dry argon by applying Schlenk techniques.[21] A perforated carbon/copper net served as support of the crystallites. Simulations of HRTEM images (multislice formalism) and of SAED patterns (kinematical approximation) were calculated with the EMS program package[22] (spread of defocus: 70 Å, illumination semiangle: 1.2 mrad). All images were recorded with a Gatan Multiscan CCD camera and evaluated (including Fourier filtering) with the program Digital Micrograph 3.6.1 (Gatan). Chemical analyses by EDX were performed in the nanoprobe and in the scanning mode of CM30ST with a Si/Li detector (Noran, Vantage System).

Acknowledgments

The authors thank R. Eger for the preparation of many samples.

[1] A. Simon, *Angew. Chem.* **1981**, *93*, 23; *Angew. Chem. Int. Ed. Engl.* **1981**, *20*, 1.
[2] a) A. Simon, Hj. Mattausch, G. J. Miller, W. Bauhofer, R. K. Kremer, in: *Handbook on the Physics and Chemistry of Rare Earths*, vol. 15 (Eds.: K. A. Gschneidner, L. Eyring), Elsevier Science Publ., Amsterdam, London, New York, Tokyo, **1991**, p. 191; b) J. D. Corbett, *J. Chem. Soc., Dalton Trans.* **1996**, 575; c) G. Meyer, *Chem. Rev.* **1988**, *88*, 93–107; d) A. Simon, Hj. Mattausch, M. Ryazanov, R. K. Kremer, *Z. Anorg. Allg. Chem.* **2006**, *632*, 919.
[3] H. G. v. Schnering, *Angew. Chem.* **1981**, *93*, 44; *Angew. Chem. Int. Ed. Engl.* **1981**, *20*, 33.
[4] J. D. Smith, J. D. Corbett, *J. Am. Chem. Soc.* **1985**, *107*, 5704.
[5] E. Warketin, R. Masse, A. Simon, *Z. Anorg. Allg. Chem.* **1982**, *491*, 323.
[6] Hj. Mattausch, A. Simon, L. Kienle, C. Hoch, C. Zheng, R. Kremer, *Z. Anorg. Allg. Chem.* **2006**, *632*, 1661.
[7] S.-J. Hwu, J. D. Corbett, *J. Solid State Chem.* **1986**, *64*, 331.
[8] O. Oeckler, L. Kienle, Hj. Mattausch, A. Simon, *Angew. Chem.* **2002**, *114*, 4431; *Angew. Chem. Int. Ed.* **2002**, *41*, 4257.
[9] O. Oeckler, Hj. Mattausch, A. Simon, *Z. Anorg. Allg. Chem.* **2005**, *631*, 3013.
[10] a) L. Kienle, Hj. Mattausch, A. Simon, *Angew. Chem.* **2006**, paper accepted for publication; b) O. Oeckler, Hj. Mattausch, A. Simon, *Z. Anorg. Allg. Chem.* **2005**, *631*, 3013.
[11] O. Oeckler, T. Weber, L. Kienle, Hj. Mattausch, A. Simon, *Angew. Chem.* **2005**, *117*, 3985; *Angew. Chem. Int. Ed.* **2005**, *44*, 3917.
[12] E. Warkentin, A. Simon, *Rev. Chim. Min.* **1983**, *20*, 488.
[13] C. Hamon, R. Marchand, Y. Laurent, J. Lang, *Bull. Soc. Fr. Min. Crist.* **1974**, *97*, 6.
[14] C. Zheng, O. Oeckler, Hj. Mattausch, A. Simon, *Z. Anorg. Allg. Chem.* **2001**, *627*, 2151.
[15] Hj. Mattausch, O. Oeckler, C. Zheng, A. Simon, *Z. Anorg. Allg. Chem.* **2001**, *627*, 1523.
[16] D. S. Dudis, J. D. Corbett, S.-J. Hwu, *Inorg. Chem.* **1986**, *25*, 3434.
[17] Hj. Mattausch, W. Schramm, R. Eger, A. Simon, *Z. Anorg. Allg. Chem.* **1985**, *530*, 43.
[18] K. Ahn, B. J. Gibson, R. K. Kremer, Hj. Mattausch, A. Stolovitz, *J. Phys. Chem. B* **1999**, *103*, 5446.
[19] A. Simon, *J. Appl. Crystallogr.* **1979**, *3*, 11.
[20] G. M. Sheldrick, SHELX97, Program package for the solution and refinement of crystal structures, Release 97–2, University of Göttingen, Germany, **1997**.
[21] P. Jeitschko, A. Simon, R. Ramlau, Hj. Mattausch, *Eur. Microscopy Microanal.* **1997**, *46*, 21.
[22] P. A. Stadelmann, *Ultramicroscopy* **1987**, *21*, 131.

Received: December 20, 2006
Published Online: March 16, 2007

